Neutrondiffraction studies of Tb2C and Dy2C in the temperature range 4–296 K

Masao Atoji

Citation: J. Chem. Phys. **75**, 1434 (1981); doi: 10.1063/1.442150
View online: http://dx.doi.org/10.1063/1.442150
View Table of Contents: http://jcp.aip.org/resource/1/JCPSA6/v75/i3
Published by the American Institute of Physics.

Neutron-diffraction studies of Tb_2C and Dy_2C in the temperature range 4–296 K[a)]

Masao Atoji

Chemistry Division, Argonne National Laboratory, Argonne, Illinois 60439
(Received 7 January 1981; accepted 20 April 1981)

Neutron power-diffraction data of the trigonal Tb_2C have been obtained and compared with our previous results (given in parentheses) for a Tb-rich Tb_2C. Significant differences were observed in the c spacing and the ferromagnetic moment, e.g., the saturation value of 7.6(8.6) Bohr magnetons, which is 84(96)% of the free-ion moment, indicating a considerable crystal-field effect. The Curie temperature (266 K) and an unusual magnetostriction along c were unchanged. The ordered-moment direction (parallel to c) has now been established unambiguously using a magnetically induced, preferential crystallite orientation in Tb_2C. A short-range ferromagnetic ordering, which coexists with the long-range ordering in Tb_2C, was analyzed anew. Dy_2C becomes ferromagnetic below 168 K, and the saturation ordered moment is 6.8 Bohr magnetons, which is 68% of the free-ion moment. A magnetically induced, preferential crystallite orientation in Dy_2C indicated that the ordered-moment direction is parallel to the [104] axis, which corresponds to the [100] axis of the high-temperature cubic modification.

I. INTRODUCTION

This study completes our current studies on the rare-earth hypocarbides REC_x which exist for RE = Sm–Lu and Y in $0.25 < x < 0.65$. The REC_x crystallized in a trigonal structure at $x \simeq 0.5$, otherwise in a NaCl-type cubic structure. The trigonal structure transforms to the cubic structure at high temperatures.[1–5] For the phase diagram involving the REC_x, the Y–C[4] and Yb–C[5] systems have been reported, showing a narrow trigonal region of roughly $0.45 < x < 0.52$ for YC_x and $0.43 < x < 0.5$ for YbC_x. Nevertheless, we frequently represent the trigonal and cubic structures by RE_2C and REC_x, respectively. The Tb_2C sample used for our previous study[6] contained 7.5 w.t% of Tb metal and hence was a Tb-rich Tb_2C with the approximate composition of $Tb_{2.1}C$.

We have studied Y_2C,[7] $Tb_{2.1}C$,[6] Ho_2C,[8] $YC_{0.28}$,[7] and $ErC_{0.6}$[9] by neutron-powder diffraction, and Y_2C[7] and $YC_{0.48}$[7] by x-ray single-crystal diffraction. This paper reports on Tb_2C and Dy_2C. All but the yttrium hypocarbides become ferromagnetic at low temperatures.[2,6–9] The reinvestigation of Tb_2C was undertaken using a Tb_2C sample of higher stoichiometry, since $Tb_{2.1}C$[6] exhibited some singular properties, such as an unusual thermal expansion of the c spacing and the ordered-moment axis of [001] in contrast with [104] in Dy_2C and Ho_2C.[8]

Lallement[2] has reported some of the physical properties of Dy_2C and $DyC_{0.4}$ as follows. The paramagnetic susceptibility of Dy_2C is characterized by a Curie–Weiss constant of 175 K, the effective Bohr magneton number of $\mu_{eff} = 11$ Bohr magnetons (μ_B), and a Curie temperature (T_c) of 177 K. The electrical resistivity showed a phase transition at 165 K in Dy_2C and at 160 K in $DyC_{0.4}$. The thermoelectric power gave the transition temperature at 140 K for Dy_2C and 135 K for $DyC_{0.4}$. Lallement[2] interpreted these properties qualitatively based on a phenomenological RKKY theory. No such measurements have been made on the physical properties of Tb_2C.

II. EXPERIMENTAL AND CRYSTALLOGRAPHIC

The carbide samples were prepared by arc-melting compressed pellets consisting of the stoichiometric mixture of filings of distilled rare-earth metal (99.9% pure) and spectroscopic-grade graphite powders. Homogeneity was ensured by repeated melting and by inversion of the ingot between melts. The product is gray metallic and can be crushed readily to a fine powder. It decomposes in moist air, liberating hydrogen and methane.[10,11] Hence, all preparatory and handling procedures were carried out in a purified argon atmosphere. Neutron and x-ray diffraction patterns showed no detectable impurity in all the samples employed. Chemical analysis gave molar ratios Tb : C = 2.00(3) : 1.00(3) for the Tb_2C sample and Dy : C = 1.94(5) : 1.00(5) for the Dy_2C sample, the number in parentheses being the estimated standard deviation of the least significant digit.

Neutron-diffraction patterns (Figs. 1 and 2) were obtained using a multipurpose diffractometer[12] set for the neutron wavelength $\lambda = 1.069$ Å (0.0716 eV). The cryomagnetic technique employed has been described in detail elsewhere.[12] The total cross section of Dy_2C (2323 b at 0.0716 eV)[13] is exceedingly large and necessitates a dilution of the Dy_2C powder sample by mixing with aluminum powder. For the packing density of 2 $g\,cm^{-3}$ in a Ti–Zr null-matrix cylindrical sample holder (1×10^{-2} m diameter), an optimum mixing ratio for attaining the maximum diffraction intensity was found to be Dy_2C : Al = 1 : 12 in molar ratio. This mixture has a linear adsorption coefficient of 2.5×10^{-2} m^{-1} and gave a set of good diffraction patterns at a scanning rate of several minutes per 0.05° step in 2θ (Fig. 2). Absorption corrections were carried out based on the method developed by Brindley[14] for mixed coarse powders. For Tb_2C, the total cross section is only 73 b[13] at 0.0716 eV, and hence the dilution of the diffraction sample was unnecessary.

Neutron reflections (Figs. 1 and 2) provided the crys-

a) Work performed under the auspices of the Office of Basic Energy Sciences, Division of Materials Science, U. S. Department of Energy.

 0021-9606/81/151434-08$01.00

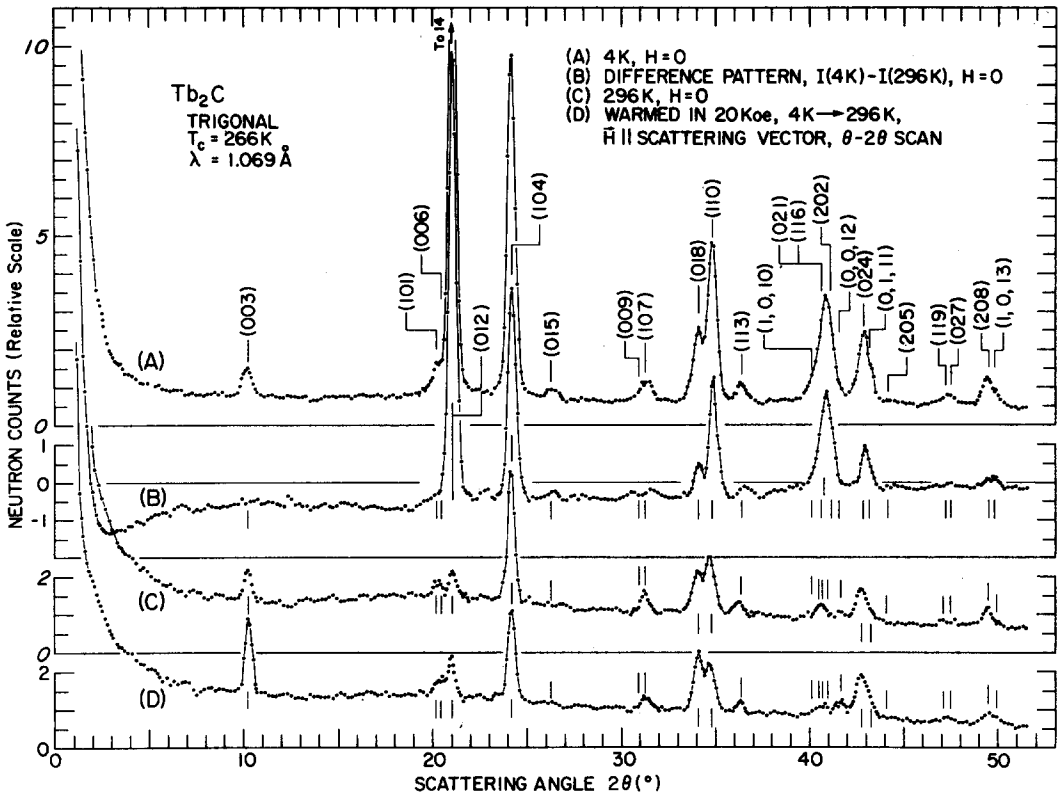

FIG. 1. Neutron-powder diffraction patterns of Tb_2C. Patterns (A) and (C) were taken at 4 and 296 K in zero magnetic field, respectively. Pattern (B) was obtained by subtracting (C) from (A), and contains only the coherent and incoherent magnetic scattering. Pattern (D) was obtained by the θ–2θ scan of the preferential crystallite orientation induced in the ferromagnetic phase by the magnetic field applied parallel to the scattering vector. The comparison between (C) and (D) indicates that the ordered-moment direction is parallel to the [104] axis.

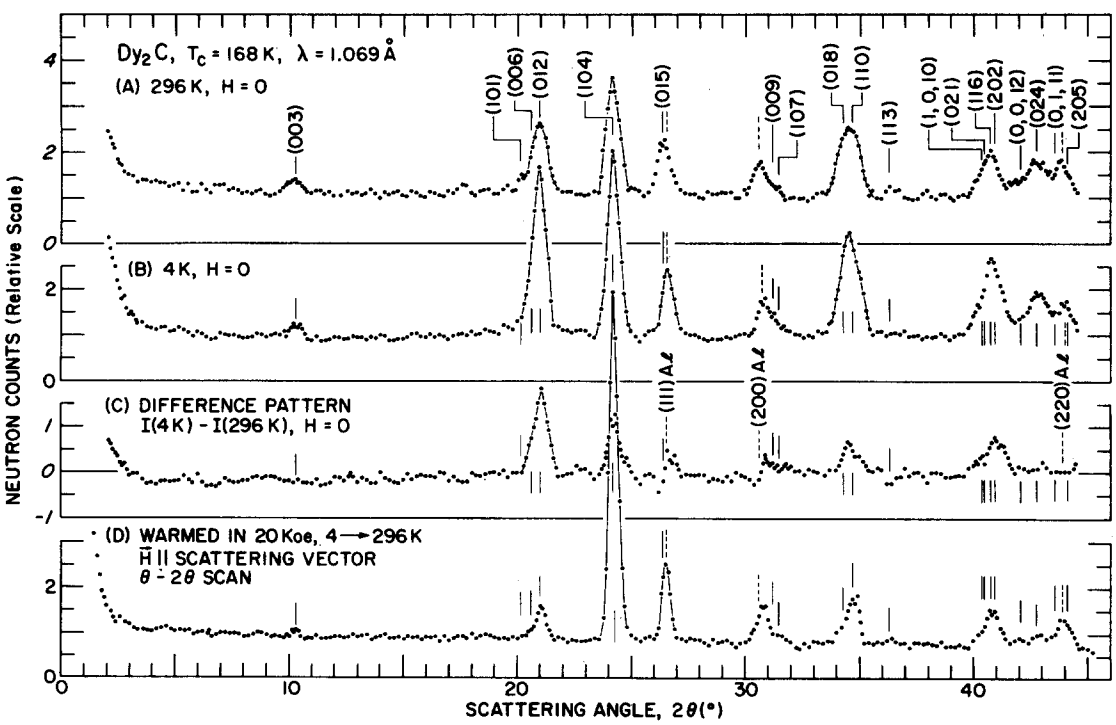

FIG. 2. Neutron-powder diffraction patterns of Dy_2C. Patterns (A) and (B) were taken at 296 and 4 K in zero magnetic field, respectively. Pattern (C) was obtained by subtracting (B) from (A) and consists of the coherent and the incoherent magnetic scattering. Pattern (D) was obtained by the θ–2θ scan of the sample, which was heated from 4 to 296 K in the magnetic field of 20 kOe with the field direction parallel to the scattering vector. The comparison between (A) and (D) indicates that the ordered moment is parallel to the [104] axis.

TABLE I. Crystal data.

Compound	$Tb_{2.1}C$		Tb_2C		Dy_2C	
Temp. (K)	4	296	4	296	4	296
$a=b$ (trigonal) (Å)	3.579(6)	3.595(6)	3.570(3)	3.584(3)	3.578(8)	3.584(6)
c (trigonal) (Å)	18.25(3)	18.19(3)	18.10(1)	18.04(1)	17.86(4)	17.89(3)
Molecular volume/RE_2C (Å^3)	67.5(2)	67.9(2)	66.6(1)	66.9(1)	66.0(3)	66.3(2)
Calc. density (g cm^{-3})	8.12(2)	8.07(2)	8.225(9)	8.188(9)	8.48(3)	8.44(2)
Temp. factor coeff. $2B$ (Å^2)	0.8(2)	3.9(5)	0.6(1)	3.0(1)	0.6(1)	2.2(2)

tal data which are summarized in Table I, where values for $Tb_{2.1}C$[6] are included for comparison. The linear thermal-expansion coefficients in 10^{-6} deg^{-1} along the a and c axes are 15, −11; 13, −11; 6, 6; and 6, 6 for $Tb_{2.1}C$,[6] Tb_2C, Dy_2C, and Ho_2C,[8] respectively. With respect to thermal expansion, $ErC_{0.6}$[9] is similar to Dy_2C and Ho_2C.[8] Hence, only $Tb_{2.1}C$ and Tb_2C exhibit an anomalous magnetostriction along the c axis. This may be correlated with the fact that the direction of the ferromagnetic moment is parallel to the c axis in Tb_2C and $Tb_{2.1}C$,[6] whereas it is parallel to [104] in Dy_2C and Ho_2C.[8] In $ErC_{0.6}$, the ordered moments are aligned parallel to the cubic [100], which corresponds to [104] of the trigonal modification.

The RE_2C structure is described by space group D_{3d}^5–$R\bar{3}m$ and the atomic coordinates $(0,0,0;\ \frac{1}{3},\frac{1}{3},\frac{1}{3};\ \frac{1}{3},\frac{2}{3},\frac{2}{3})\pm(0,0,z)$ for RE atoms and $\pm(0,0,0)$ for carbon atoms. The intensity analysis gave $z=0.2593(6)$ for Tb_2C (unchanged from $Tb_{2.1}C$)[6] and 0.2575(8) for Dy_2C. The observed and calculated nuclear intensities at 296 K are listed in Tables II and III, where the agreement factor $R=\sum|I_0-I_c|/\sum I_0$ is 3.0% for Tb_2C and 0.96% for Dy_2C. The scattering lengths used[15] were $b(\mathrm{Tb})=0.76$, $b(\mathrm{Dy})=1.69$, and $b(\mathrm{C})=0.665$, all in 10^{-14} m.

III. MAGNETIC STRUCTURE

The neutron diffraction pattern at temperatures below the Curie temperature exhibited varying growths of peaks at the nuclear-reflection sites without the generation of new reflections. This verifies the onset of the ferromagnetic ordering (Figs. 1 and 2). No peak broadening was observed in the temperature range 4–296 K, implying that the moment alignment is not a HoN-type retarded-spiral structure.[15]

Subsequently, the magnetic structure was satisfactorily interpreted based on a uniaxial, commensurate-lattice formula

$$I_{\mathrm{calc}}(\mathrm{mag})=\left(\frac{e^2\gamma}{2mc^2}\right)^2 jLf_m^2F_m^2M^2\exp\left[-2B\left(\frac{\sin\theta}{\lambda}\right)^2\right]\times[\sin^2\psi-\tfrac{1}{2}(3\sin^2\psi-2)\sin^2\phi],$$

where the reported equation[16] has been modified so that each variable can be evaluated independently; γ is the neutron magnetic moment in nuclear Bohr magnetons; j is the multiplicity factor; L is the Lorenz factor; f_m is the magnetic-form factor[17]; F_m is the magnetic-structure factor and is equal to $\cos 2\pi lz$; M is the ordered magnetic moment; ψ is the angle between the c axis and the scattering vector; and ϕ is the angle between the c axis and the moment direction. The direction of the basal-plane component of the moment cannot be determined by the neutron-powder method.[16] Moreover, the calculated intensities are relatively insensitive to the ϕ variation.

Consequently, the direction of the ordered moment was determined using the preferential crystallite orientation induced by the applied magnetic field.[18] The net moment of the crystallite tends to align in the direction of the applied magnetic field. The resultant preferential orientation can be determined by a θ–2θ scan, with the magnetic field applied parallel to the scattering vector. However, the effect of the preferred orientation on the nuclear intensity is quite different from that on the magnetic intensity. Hence, the preferred orientation is induced in the ferromagnetic phase, but the intensity data are collected in the paramagnetic phase in order to eliminate the magnetic intensity.

In practice, since vibrational disturbances during experimental procedures can alter the powder packing,

TABLE II. Observed and calculated nuclear intensities in 10^{-26} m per 0.5 Tb_2C at 296 K.

Indices	I_{calc}		I_{obs}	Indices	I_{calc}		I_{obs}
003	26.9		20.0	1,0,10	1.8		
101	7.6			021	1.6		
006	4.3	27.0	27.0	116	5.6	17.5	17.4
012	15.0			202	3.4		
104	71.9		71.7	0,0,12	5.1		
015	0.7		<0.8	024	19.7		
009	0.0	14.3	14.8	0,1,11	10.3	30.2	30.3
107	14.3			205	0.2		
018	29.8	63.2	62.9	119	0.1	5.4	5.4
110	33.4			027	5.3		
113	10.9		10.8	208	12.2	12.6	12.5
				1,0,13	0.4		

TABLE III. Observed and calculated nuclear intensities in 10^{-26} m per 0.5 Dy_2C at 296 K.

Indices	I_{calc}		I_{obs}	Indices	I_{calc}		I_{obs}
003	40		42	113	18		17
101	6			1,0,10	29		
006	50	213	212	021	1	138	139
012	157			116	70		
104	255		255	202	38		
015	0		0	0,0,12	20		
009	2	31	27	024	75	119	118
107	29			0,1,11	25		
018	111	233	234	205	0		
110	122						

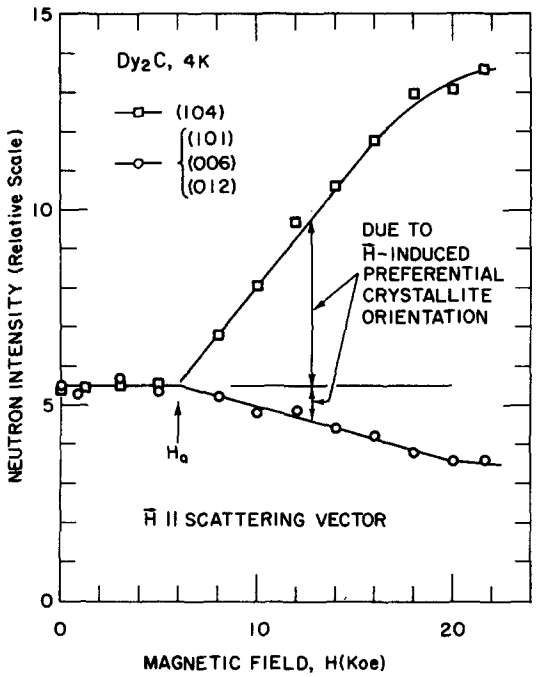

FIG. 3. The intensity of the (104) reflection and that of the peak consisting of (101), (006), and (012) of Dy_2C at 4.2 K as a function of the magnetic field applied parallel to the scattering vector. The magnetic field of about H_a=6 kOe is needed to overcome the steric hindrance in the powder packing for starting the orientation of the crystallites. When H increases beyond H_a, the (104) intensity increases due to the preferential crystallite orientation. On the other hand, because of the specific moment alignment, the intensity of the composite peak decreases as H increases.

TABLE IV. Observed and calculated intensities of nuclear and magnetic reflections in 10^{-26} m per 0.5 Tb_2C at 4 K. The ferromagnetic moments are aligned parallel to the c axis.

Indices	I_{calc} (nucl)	I_{calc} (mag)	I_{calc} (total)	I_{obs}
003	27.5	0	27.5	27.2
101	8.1	1.1		
006	4.6	0	284.5	290.0
012	16.0	254.7		
104	78.6	130.7	209.3	207.7
015	0.8	7.8	8.5	8.5
009	0.0	0	23.1	23.1
107	16.6	6.4		
018	35.8	21.2	57.0	56.3
110	39.9	71.1	111.0	109.6
113	13.3	3.5	16.8	16.1
1,0,10	2.3	8.0		
021	2.1	0.2		
116	7.2	55.3	125.4	125.9
202	4.4	39.4		
0,0,12	6.7	0		
024	25.9	30.0		
0,1,11	13.8	2.7	74.9	75.0
205	0.3	2.2		
119	0.1	7.0	17.4	17.5
027	7.5	2.8		
208	17.6	11.2	31.0	29.2
1,0,13	0.6	1.6		

TABLE V. Observed and calculated intensities of nuclear and magnetic reflections in 10^{-26} m^2 per 0.5 Dy_2C at 4 K. The ferromagnetic moments are aligned parallel to the [104] axis (ϕ=55.2°).

Indices	I_{calc} (nucl)	I_{calc} (mag)	I_{calc} (total)	I_{obs}
003	40.4	5.3	46	39
101	6.3	0.4		
006	51.6	51.4	430	432
012	163.9	156.5		
104	270.0	107.4	377	373
015	0.2	4.9	5	5
009	1.8	3.2	42	40
107	31.5	5.8		
018	124.9	37.0	340	345
110	137.5	40.7		
113	20.1	1.4	22	22
1,0,10	34.6	20.4		
021	1.6	0.1	253	253
116	82.3	45.7		
202	44.6	24.1		
0,0,12	24.0	7.3		
024	89.5	20.3	177	178
0,1,11	29.8	4.9		
205	0.1	1.0		

the applied magnetic field is kept on in the heating process. The magnetic field should be stronger than H_a (Fig. 3) to overcome the steric hindrance in the powder packing. On the other hand, the magnetic field should be smaller than that inducing the orientation of the magnetic domain or the modulation of the magnetic structure. Within these two limits, the magnetic field should be as strong as possible for obtaining the largest attainable preferred orientation. To comply with these criteria, the intensity of the representative magnetic reflection must be measured as a function of the magnetic field at $T \ll T_c$. An example of such a measurement for Dy_2C is shown in Fig. 3, which demonstrates that a conveniently available high field of 20 kOe is appropriate for our experiment. A similar conclusion was also obtained for Tb_2C. Diffraction intensities for the preferred crystalline orientation in the hexagonal symmetry have been formulated by Pesonen *et al.*[19]

The diffraction patterns of the modulated crystallite orientation thus obtained showed that the direction of the ferromagnetic moment is parallel to the c axis (ϕ=0) in Tb_2C and to the [104] axis (ϕ=55.2°) in Dy_2C. The [104] axis in the trigonal system corresponds to the [100] axis in the cubic modification. The observed and calculated values for the nuclear and magnetic intensities at 4 K are tabulated for Tb_2C and Dy_2C in Tables IV and V, where the agreement factors are 1.3% and 1.2%, respectively. The ordered magnetic moment of Tb_2C at 4 K is 7.6(1) μ_B, which is 84% of the free-ion moment of 9 μ_B. In Dy_2C at 4 K, it is 6.8(1) μ_B, which is 68% of the free-ion moment of 10 μ_B. In all RE_2C, the ordered moment is well saturated at 4 K and indicates a considerable crystal-field effect.

In the previous analysis of $Tb_{2.1}C$,[6] the ordered-moment direction was chosen as approximately parallel to the c axis, since, otherwise, the moment value exceeds the free-ion value unreasonably. The field-in-

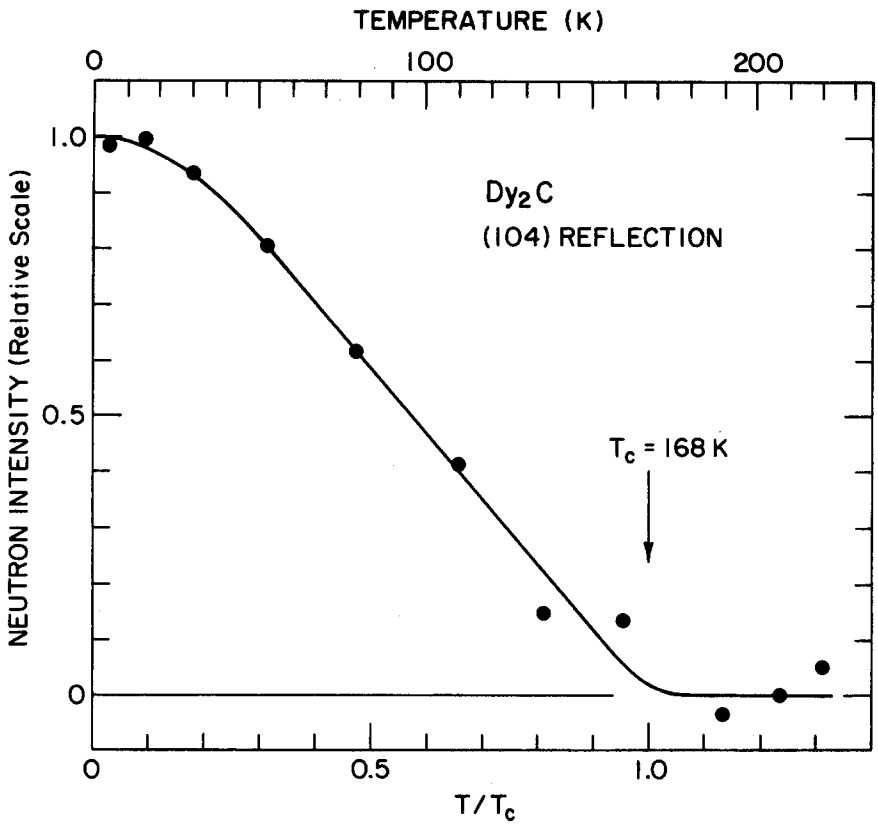

FIG. 4. Determination of the Curie temperature of Dy_2C by the temperature dependence of the magnetic intensity of the (104) reflection.

duced preferential crystallite-orientation method was not applied to $Tb_{2.1}C$, because of probable interference from the Tb-metal impurity, which becomes ferromagnetic below 245 K.[6] Despite these uncertainties, the ordered-moment direction in $Tb_{2.1}C$ is probably parallel to the c axis, since both Tb_2C and $Tb_{2.1}C$ exhibit the same unique magnetostriction.

The temperature dependency of the spontaneous magnetization in Tb_2C is essentially the same as that in $Tb_{2.1}C$.[6] For Dy_2C, the temperature dependency of the integrated intensity of the (104) reflection is shown in Fig. 4, which gives $T_c = 168(2)$ K, in good agreement with Lallement's results.[2] The reduced spontaneous magnetic moment $M(T)/M(O)$ is plotted as a function of the reduced temperature T/T_c for Tb_2C, Dy_2C, and Ho_2C in Fig. 5, where $M(T)$ is the ordered moment at T K. The Tb_2C and Ho_2C curves are represented closely by $M(T) = M(O)\,[1-(T/T_c)^n]$ with $n = 2$ and $\frac{2}{3}$, respectively. The Dy_2C moments appear to follow the Tb_2C curve, but suffer from large experimental uncertainties. In all these RE_2C cases, the Brillouin curve for $(g-1)J$ is definitely not in accordance with the observed value.

Concerning the magnetic diffuse scattering, the $Tb_{2.1}C$ data were not analyzed because of an ambiguity due to the Tb-metal impurity. Also, the diffuse scattering of Dy_2C was not studied because of large attenuation corrections. The Tb_2C experiments provided excellent diffuse scattering data (Fig. 6) which were analyzed using a first-order approximation of the short-range-order formula[20]

$$\frac{d\sigma}{d\omega} = \frac{2}{3}\left(\frac{e^2\gamma}{2mc^2}\right)^2 \mu_{eff} f_m^2 \left(1 - \frac{2\mu_{eff}^2}{3kT}\sum_n J_n z_n \frac{\sin X_n}{X_n}\right) ,$$

where $d\sigma/d\omega$ is the differential scattering cross section in $b/sr/Tb^{3+}$, the first term represents the paramagnetic scattering, and the second term represents the short-range-order effect; γ is the neutron magnetic moment in nuclear Bohr magnetons; J_n is proportional to the exchange interaction between the given atom and the nth neighboring atom; z_n is the number of nth neighbors; and $X_n = 4\pi r_n(\sin\theta)/\lambda$, where r_n is the distance to the nth neighbor. The data-reduction process for obtaining the paramagnetic scattering has been explained in detail elsewhere.[21]

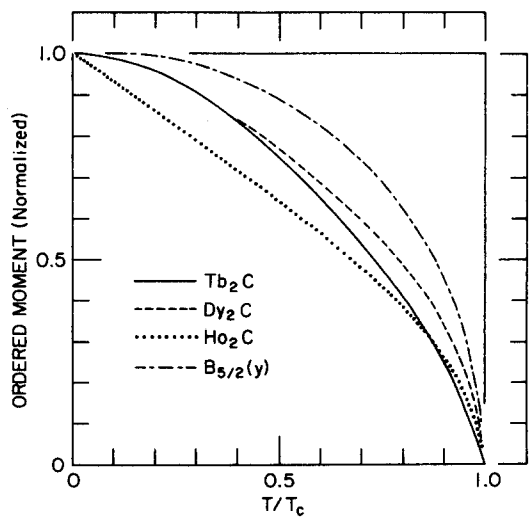

FIG. 5. Reduced magnetic moment as a function of reduced temperature T/T_c for Tb_2C, Dy_2C, and Ho_2C. For comparison, the Brillouin curve for $(g-1)J = \frac{5}{2}$ of the free Dy^{3+} ion is shown by a broken line.

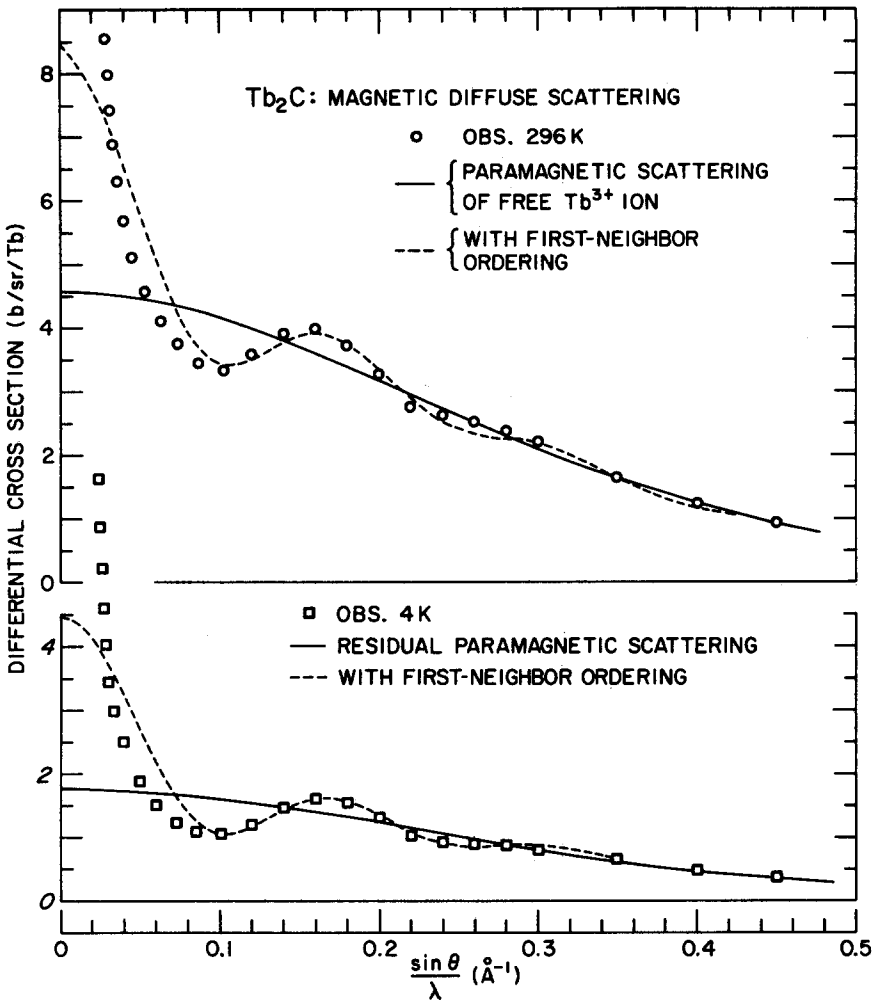

FIG. 6. Observed diffuse magnetic-scattering cross sections of Tb_2C at 296 and 4 K are given by open circles and open squares, respectively. The calculated curve for the incoherent magnetic scattering in the disordered magnetic moments is shown by a solid line. The calculated scattering in the disordered moments with a ferromagnetic first-neighbor short-range ordering is given by a broken line.

The median curve of the observed data at 296 K was fitted using $\mu_{eff} = 9.7(2)\ \mu_B$, which agrees with the $\mu_{eff} = 9.72\ \mu_B$ of the free Tb^{3+} ion. From the wavy modulation of the scattering curve at 296 K, a first-neighbor ferromagnetic short-range-order parameter $J_1 = -0.422k$ was deduced. The wavy modulation persists down to 4 K, inferring that the short-range ferromagnetic ordering coexists with the long-range ferromagnetic ordering.[22] The median curve of the diffuse scattering at 4 K was interpreted as a disordered-moment scattering with $\mu_{eff} = 6\ \mu_B$, which corresponds to $[(\mu_{eff}$ for the free ion$)^2 - ($ordered moment$)^2]^{1/2} = (9.72^2 - 7.6^2)^{1/2} = 6.06\ \mu_B$. Although no unique curve fit was obtained in the short-range-order terms, a first-neighbor interaction curve is shown in Fig. 4 for illustration using a ferromagnetic $J_1 = -0.028k$. A very strong intensity in the vicinity of $\theta = 0$ consists of all the ferromagnetic short-range orderings at the maximum positive values and an intense coherent ferromagnetic reflection at $h = k = l = 0$. In the previous $Tb_{2.1}C$ study,[6] this peak at $\theta = 0$ was incorrectly interpreted as a small-angle scattering due to a magnetic structure having a large superlattice.

IV. DISCUSSION

The trigonal RE_2C structure (an anti-$CdCl_2$-type) is composed of the stacking of the hexagonal layers along the c axis in the sequence AcBvCbAvBaCv..., where A, B, and C are RE layers; a, b, and c are carbon layers; and v signifies a vacant layer (see Fig. 4 of Ref. 7). Hence, the RE_2C structure may be viewed as the cubic closest packing of the RE atoms interleaved alternately by the filled and vacant carbon layers. The perpendicular distance between the adjacent RE layers across the carbon layer is much shorter than that across the vacant layer as indicated by 2.68(2) and 3.35(2) Å in Tb_2C, and 2.71(3) and 3.25(3) Å in Dy_2C, respectively, all at 4 K. In a transition-metal carbide, this relation is reversed, e.g., in α-Ta_2C, which has an anti-CdI_2 structure (a hexagonal close-packed analog of the anti-$CdCl_2$ structure), the perpendicular distances between the adjacent metal layers are 2.505 Å across the carbon layer and 2.432 Å across the vacant layer.[23]

The metal–metal bond distances (in Å) in Tb_2C are Tb(I)–3Tb(III) = 3.381(9) across the carbon layer, Tb(I)–6Tb(II) = 3.570(3) within the layer, and Tb(I)–3Tb(IV) = 3.94(2) across the vacant layer. In Dy_2C, Dy(I)–3Dy(III) = 3.41(1), Dy(I)–6Dy(II) = 3.578(8), and Dy(I)–3Dy(IV) = 3.85(3). The RE(I)–RE(III) distance is considerably *shorter* than the bonding distance of 3.56 Å in the Tb metal and 3.55 Å in the Dy metal.[24] Conversely, the Ta–Ta bonding distances of 3.02 and 3.08 Å in α-Ta_2C are *longer* than the bond distances of 2.86 Å in the Ta metal.[23] The carbon atom is bonded to the

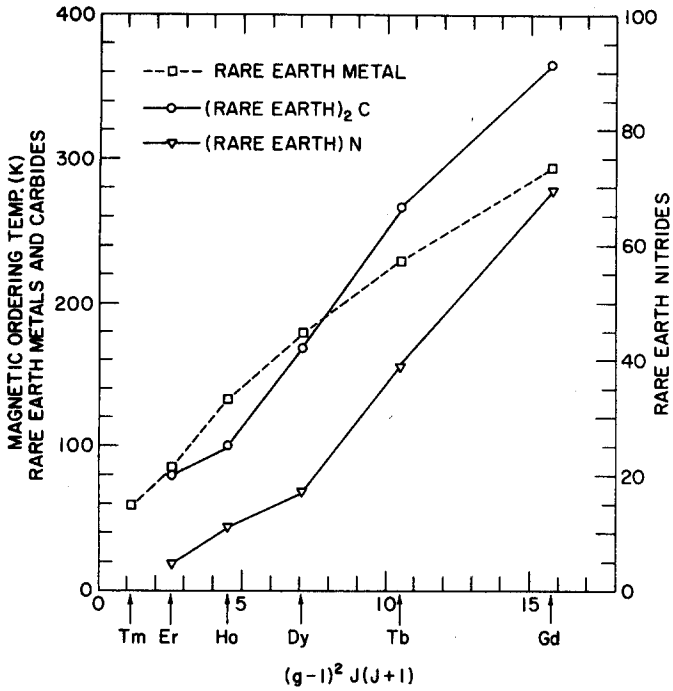

FIG. 7. Magnetic order–disorder temperatures of the metals, the hypocarbides, and the nitrides of the heavy rare earths as a function of the DeGenne parameter.

rare-earth atoms with C–6RE = 2.458(6) in Tb_2C and 2.470(9) Å in Dy_2C. These C–RE distances are comparable to 2.458(6) and 2.400(3) Å in TbC_2[21] and DyC_2,[24] respectively.

Similarly, the lattice parameter of REC_x decreases as the carbon content increases. In Tb_2C, although the nonstoichiometric range is very narrow, the above relation is more pronounced in c than in a (Table I). This is expected in the RE_2C-type layer-stacking structure.[7] The bonding characteristics described above suggest that the carbon atom in the rare-earth hypocarbide provides a considerable amount of bonding electrons to the s–d bond orbitals among the rare-earth atoms. In the transition-metal carbide, the lattice parameter increases as the carbon content increases. This means that the carbon atom provides its bonding electrons mostly to the carbon–metal bonds, but much less to the metal–metal bonds.

The magnetic order–disorder transition temperatures (T_t) of the RE metals (hexagonal closest packing),[25] RE_2C,[2,8,9] and REN (cubic NaCl-type)[26] for RE = Gd–Tm are plotted as a function of DeGenne factor $G = (g-1)^2 \times J(J+1)$ in Fig. 7. The T_t represents the antiferromagnetic transition temperature for the RE metals (RE = Tb–Tm) and the ferromagnetic transition temperature for the Gd metal, RE_2C, and REN. In a simple molecular-field approximation $T_t = J_e G$, where J_e is proportional to the exchange energy, provided that the anisotropy and crystal-field effects are insignificant. The J_e values are approximately 24, 25, and 2.9 for the RE metals, RE_2C, and REN, respectively. Hence, the exchange energy is about the same in the RE metals and RE_2C, but is much smaller in REN.

The difference $\Delta T_t = (T_t$ of the RE metal$) - (T_t$ of the $RE_2C)$, is progressively smaller in the order RE = Gd – Ho. The ΔT_t values are 36, –8, and –30 K for RE = Tb, Dy, and Ho, respectively, and can be correlated to the strengths of the RE(I)–RE(III) bonds, which are 5%, 4% and 3% shorter than the bond distances in the respective RE metals. The above relations are interpreted as follows. In Gd_2C, both the exchange interaction and the metal–metal bonds are considerably stronger than those in the Gd metal. These differences become smaller in the heavier rare earths, and the relation is reversed in RE = Ho (Fig. 7). The ordered-moment directions in Tb_2C, Dy_2C, and Ho_2C are [001], [104], and [104], which correspond to [111], [100], and [100] in the cubic modification, respectively. In REN, the ordered-moment directions are similarly [111], [100], and [100] for RE = Tb, Dy, and Ho, respectively.[15] This indicates that the energy-level scheme of the RE_2C is analogous to that of the REN.[26] However, since T_t of the RE_2C is much higher than that of the REN, the crystal-field effect should be much smaller in the RE_2C than in the REN. This seems reasonable, since the ionic bonding character[27] of the RE_2C is much weaker than that of the REN and the lattice spacing of the RE_2C is larger than that of the REN.

[1] F. H. Spedding, K. Gschneidner, Jr., and A. H. Daane, J. Am. Chem. Soc. 80, 4499 (1958).
[2] R. Lallement, Centre d' Etudes Nucleaires de Fonteney-Aux-Roses Rapport, CEA-R 3043 (1966).
[3] G. L. Bacchella, P. Meriel, M. Pinot, and R. Lallement, Bull. Soc. Fr. Mineral. Cristallogr. 89, 226 (1966).
[4] O. N. Carlson and W. M. Paulson, Trans. Metall. Soc. AIME 242, 846 (1968).
[5] J. M. Haschke and H. A. Eick, J. Am. Chem. Soc. 92, 1526 (1970).
[6] M. Atoji, J. Chem. Phys. 51, 3872 (1969).
[7] M. Atoji and M. Kikuchi, J. Chem. Phys. 51, 3863 (1969); ANL Report ANL-7441 (1968).
[8] M. Atoji, J. Chem. Phys. 74, 1893 (1981).
[9] M. Atoji, J. Chem. Phys. 74, 1898 (1981).
[10] H. J. Svec, J. Capellen, and F. E. Saafeld, J. Inorg. Nucl. Chem. 26, 721 (1964).
[11] J. S. Anderson, N. J. Clark, and I. J. McColm, J. Inorg. Nucl. Chem. 30, 105 (1968).
[12] M. Atoji, Nucl. Instrum. Methods 35, 13 (1965); ANL Report ANL-6920 (1964).
[13] M. D. Goldberg, S. F. Mughabghab, S. N. Purohit, B. A. Magurno, and V. M. May, "Neutron Cross Sections," Vol. IIC, "Z = 61 to 87," BNL Report BNL-325, 2nd ed. Supp. No. 2 (1966).
[14] G. W. Brindly, Philos. Mag. 36, 347 (1945).
[15] H. R. Child, M. K. Wilkinson, J. W. Cable, W. C. Koehler, and E. O. Wollan, Phys. Rev. 131, 911 (1963).
[16] G. E. Bacon, *Neutron Diffraction* (Clarendon, Oxford, 1975), 3rd ed.
[17] M. Blume, A. J. Freeman, and R. E. Watson, J. Chem. Phys. 37, 1245 (1952); 41, 1878 (1964).
[18] M. Atoji, I. Atoji, C. Do-Dinh, and W. E. Wallace, J. Appl. Phys. 44, 5096 (1973).
[19] A. Pesonen, M. Jarvinen, and K. Kurki-Suonio, Phys. Fenn. 8, 81 (1973).
[20] M. Slotnik, Phys. Rev. 83, 1226 (1951).
[21] M. Atoji, J. Chem. Phys. 35, 1950 (1961); 46, 1891 (1967).
[22] G. T. Trammell, Phys. Rev. 131, 932 (1963).

[23]A. L. Bowman, T. C. Wallace, J. L. Yarnell, R. G. Wenzel, and E. K. Storm, Acta Crystallogr. 19, 6 (1965).
[24]M. Atoji, J. Chem. Phys. 48, 3384 (1968).
[25]B. Cogblin, *The Electronic Structure of Rare-Earth Metals and Alloys: The Magnetic Heavy Rare-Earths* (Academic, New York, 1977).
[26]F. Hullinger, in *Handbook on the Physics and Chemistry of Rare Earths*, edited by K. A. Gschneidner, Jr. and LeRoy Eyring (North-Holland, Amsterdam, 1979), Vol. 4, Chap. 33.
[27]L. Pauling, *The Nature of the Chemical Bond*, 3rd ed. (Cornell University, Ithaca, 1960).